Proton Migration and Defect Interactions in the $CaZrO_3$ Orthorhombic Perovskite: A Quantum Mechanical Study

M. Saiful Islam,*,† R. Andrew Davies,† and Julian D. Gale‡

Department of Chemistry, University of Surrey, Guildford GU2 7XH, U.K., and Department of Chemistry, Imperial College of Science, Technology and Medicine, South Kensington, London SW7 2AY, U.K.

Received January 3, 2001. Revised Manuscript Received March 20, 2001

Quantum mechanical techniques based on density functional theory have been used to investigate the mechanism and energetics of proton transport in the perovskite-structured $CaZrO_3$. The calculations demonstrate that the observed orthorhombic crystal structure (comprised of tilting $[ZrO_6]$ octahedra) is reproduced accurately. Quantum mechanical molecular dynamics simulations confirm that the diffusion mechanism involves proton transfer from one oxygen ion to the next (Grötthuss-type mechanism) and also indicate the importance of the vibrational dynamics of the oxygen sublattice. For each hopping event, the oxygen−oxygen distance contracts to about 2.4−2.5 Å so as to assist proton transfer. By exploration of the energy profiles for proton transfer, a very low energy barrier is found for the O(1)−O(1) interoctahedra path. However, long-range proton conduction may involve O(1)−O(2) proton transfer as the rate-limiting step with a calculated energy barrier of 0.74 eV. Binding energies for hydroxyl−dopant pairs involving Ga^{3+}, Sc^{3+}, and In^{3+} dopant ions are predicted to be favorable and are compatible with observed proton "trapping" energies from previous muon spin relaxation and quasi-elastic neutron scattering experiments.

1. Introduction

Ceramic oxides with the perovskite structure have received considerable attention as solid-state proton conductors,[1−4] with a range of promising electrochemical applications including fuel cells, gas sensors, and hydrogen pumps. Most attention has focused on cerates $(ACeO_3)$[5−8] and zirconates $(AZrO_3)$,[9−12] which possess varying levels of proton conductivity. For example, a commercial hydrogen sensor has been developed based upon doped $CaZrO_3$ as the proton-conducting electrolyte, which exhibits high chemical and thermal stability.[13] These materials are typically doped with lower valent (acceptor) cations to form oxygen vacancies as charge-compensating defects. By means of treatment in water vapor, these vacancies may be replaced by protons, which reside on oxygen ions to give OH^- ions.

It is acknowledged that the macroscopic behavior of materials is often controlled by fundamental mechanisms acting on the microscopic scale. However, the information derived from most conductivity or diffusion experiments is not sufficient to identify the atomistic transport mechanism, especially in the case of a proton where the influence of quantum effects may be significant. By employing atomistic simulation and X-ray absorption (EXAFS) techniques, we have already obtained valuable microscopic information on defect structures and proton incorporation in perovskite-type cerates and zirconates.[14,15] This paper will amplify such knowledge by investigating proton diffusion in orthorhombic $CaZrO_3$ using quantum mechanical techniques. We employ static and dynamical simulations, based upon density functional theory (DFT), which are well suited to probing electronic structures and migration energetics.

* To whom correspondence should be addressed. E-mail: m.islam@surrey.ac.uk.

† University of Surrey.

‡ Imperial College of Science, Technology and Medicine.

(1) (a) Iwahara, H. *Solid State Ionics* **1995**, *77*, 289. (b) Iwahara, H. *Solid State Ionics* **1999**, *125*, 271.

(2) (a) Kreuer, K. D. *Chem. Mater.* **1996**, *8*, 610. (b) Kreuer, K. D. *Solid State Ionics* **1999**, *125*, 285.

(3) (a) Norby, T.; Larring, Y. *Curr. Opin. Solid State Mater. Sci.* **1997**, *2*, 593. (b) Norby, T. *Solid State Ionics* **1999**, *125*, 1.

(4) Nowick, A. S.; Du, Y.; Liang, K. C. *Solid State Ionics* **1999**, *125*, 303.

(5) (a) Yajima, T.; Iwahara, H. *Solid State Ionics* **1992**, *50*, 281. (b) Liu, J. F.; Nowick, A. S. *Solid State Ionics* **1992**, *50*, 131.

(6) (a) Slade, R. C. T.; Flint, S. D.; Singh, N. *J. Mater. Chem.* **1995**, *4*, 509. (b) Kreuer, K. D.; Dippel, T.; Baikov, Y. M.; Maier, J. *Solid State Ionics* **1996**, *86−88*, 613.

(7) (a) Shima, D.; Haile, S. M. *Solid State Ionics* **1997**, *97*, 443. (b) Kunstler, K.; Lang, H. J.; Maiwald, A.; Tomandl, G. *Solid State Ionics* **1998**, *107*, 221. (c) Goretta, K. C.; Park, E. T.; Guan, J.; Balachandran, U.; Dorris, S. E.; Routbort, J. L. *Solid State Ionics* **1998**, *111*, 295.

(8) (a) Phillips, R. J.; Bonanos, N.; Poulsen, F. W.; Ahlgren, E. O. *Solid State Ionics* **1999**, *125*, 389. (b) Knight, K. S. *Solid State Ionics* **2000**, *127*, 43. (c) Qi, X.; Lin, Y. S. *Solid State Ionics* **2000**, *130*, 149.

(9) (a) Labrincha, J. A.; Frade, J. R.; Marques, F. M. B. *Solid State Ionics* **1993**, *61*, 71. (b) Schober, T.; Friedrich, J.; Condon, J. B. *Solid State Ionics* **1995**, *77*, 175.

(10) (a) Yugami, H.; Matsuo, S.; Ishigame, M. *Solid State Ionics* **1995**, *77*, 195. (b) Ryu, K. H.; Haile, S. M. *Solid State Ionics* **1999**, *125*, 355. (c) van Rij, L.; Winnubst, L.; Jun, L.; Schoonman, J. *J. Mater. Chem.* **2000**, *10*, 2515.

(11) Schober, T.; Bohn, H. G. *Solid State Ionics* **2000**, *127*, 351.

(12) Gross, B.; Engeldinger, J.; Grambole, D.; Hermann, F.; Hempelmann, R. *Phys. Chem. Chem. Phys.* **2000**, *2*, 297.

(13) (a) Yajima, T.; Koide, K.; Takai, H.; Fukatsu, N.; Iwahara, H. *Solid State Ionics* **1995**, *79*, 333. (b) Fukatsu, N.; Kurita, N.; Koide, K.; Ohashi, T. *Solid State Ionics* **1998**, *115*, 219.

(14) (a) Davies, R. A.; Islam, M. S.; Gale, J. D. *Solid State Ionics* **1999**, *126*, 323. (b) Davies, R. A.; Islam, M. S.; Chadwick, A. V.; Rush, G. E. *Solid State Ionics* **2000**, *130*, 115.

(15) (a) Islam, M. S. *J. Mater. Chem.* **2000**, *10*, 1027. (b) Glöckner, R.; Islam, M. S.; Norby, T. *Solid State Ionics* **1999**, *122*, 145.

10.1021/cm010005a CCC: $20.00
Published on Web 05/12/2001

Our study focuses on the orthorhombic perovskite phase of $CaZrO_3$, which extends previous computational studies of ideal cubic structures of cerates,[16,17] zirconates,[18,19] and titanates.[17,19−21] For example, recent simulations of Münch et al.[19,20] found that the proton locally "softens" the cubic lattice and that hydroxyl reorientation is much faster than the proton-transfer step. The present study attempts to examine how the OH configuration and the proton migration mechanism are affected by the local environment and the appreciable distortion of the ZrO_6 octahedra of orthorhombic $CaZrO_3$. Because cation acceptor doping is crucial to proton incorporation, interactions between the dopant and the hydroxyl ion are also considered, a topic that has been paid limited attention.

2. Simulation Techniques

Recent developments have made ab initio techniques powerful tools for the accurate calculation of materials' properties. In this section, we will give a brief account of the computational methods because more detailed reviews are given elsewhere.[22−24]

In general, the total energy and the forces on all of the nuclei are obtained by solving Schrödinger's equation at some level of approximation to determine the electronic ground state. The calculations here are performed within the framework of DFT, with the exchange-correlation energy being treated using the generalized-gradient approximation (GGA) of Perdew et al.[25] It has been documented that gradient corrections offer significant improvements in the treatment of hydrogen bonds and proton transfer.[26] However, it is still recognized that there are likely to be uncertainties in the activation energies due to the limitations of the present day functionals. The particular implementation of DFT employed here combines a plane-wave basis set with the total energy pseudopotential method, as embodied in the CASTEP code,[22] which is ideally suited to calculations on periodic systems. This approach assumes that the tightly held core electrons are in the same states as in the free atoms, with the pseudopotential representing the interaction between valence electrons and the atomic cores via a nonlocal potential.

Our simulations on $CaZrO_3$ are based upon ultrasoft pseudopotentials of the form due to Vanderbilt,[27] with an ultrasoft pseudopotential derived by Pickard[28] for hydrogen. The reference atomic valence configurations used to construct the pseudopotentials are as follows: H ($1s^12p^0$), O ($2s^22p^4$), Ca ($3s^23p^64s^2$), and Zr ($4s^24p^64d^25s^2$). For all of the simulations, we used a supercell containing 20 atoms of the bulk structure (corresponding to $Ca_4Zr_4O_{12}$) repeated periodically in all directions. The Brillouin zone was sampled according to the Monkhorst−Pack scheme[29] using a $2 \times 1 \times 2$ mesh, which leads to two symmetry unique k points when allowing for the inversion symmetry of the Patterson group. A plane-wave cutoff of 560 eV was selected after monitoring of the convergence of the unit cell lattice parameters and atomic coordinates with respect to the number of plane waves, as well as the binding energy when protons were incorporated into the system. It is worth noting that DFT pseudopotential techniques of this kind have been applied successfully to other oxides including studies of bulk defects,[30] molecular absorption on surfaces,[26] and lithium intercalation.[31,32]

3. Results and Discussion

3.1. $CaZrO_3$ Structure and Proton Position. The starting point for this study, prior to the introduction of the proton, was the simulation of the equilibrium bulk structure. The perovskite structure of $CaZrO_3$ is built upon a framework of corner-linked ZrO_6 octahedra with the calcium ion in a 12-coordinate site. The orthorhombic phase (of space group *Pcnm*)[33] is observed from room temperature up to 2023 K,[34] covering typical operating temperatures for electrochemical use. The orthorhombic structure exhibits significant tilting of the octahedra from the ideal cubic configuration with Zr−O−Zr angles of about 146° and two inequivalent oxygen positions (O(1) apical and O(2) equatorial).

The calculated and experimental lattice parameters, atomic positions, and bond lengths are listed in Table 1. Examination of the values shows good agreement between experimental and simulated structures, with the deviation in the cell parameters and bond lengths being less than 0.5%. As expected for nonlocal DFT, the volume is slightly overestimated. Nevertheless, the appreciable tilting of the ZrO_6 octahedra (and the corresponding Zr−O−Zr bending) is correctly reproduced. The simulation of the structure, therefore, provides an accurate starting point for the subsequent calculations.

Protons are introduced into doped perovskites by treatment with water vapor, whereby oxygen vacancies are filled by hydroxyl species ($OH_O^{\bullet}$); the proton is, therefore, considered to be closely associated with an oxygen ion to form the hydroxyl group. However, in the evaluation of the ion transport properties, it is important to know the precise location of the proton, which can be difficult to extract from conventional diffraction

(16) Münch, W.; Seifert, G.; Kreuer, K. D.; Maier, J. *Solid State Ionics* **1996**, *86−88*, 647.
(17) (a) Shimojo, F.; Hoshino, K.; Okazaki, H. *Solid State Ionics* **1998**, *113−115*, 319. (b) Shimojo, F.; Hoshino, K.; Okazaki, H. *J. Phys. Condens. Matter* **1998**, *10*, 285.
(18) Yoshino, M.; Nakatsuka, K.; Yukawa, H.; Morinaga, M. *Solid State Ionics* **2000**, *127*, 109.
(19) Münch, W.; Seifert, G.; Kreuer, K. D.; Maier, J. *Solid State Ionics* **1997**, *97*, 39.
(20) Münch, W.; Kreuer, K. D.; Seifert, G.; Maier, J. *Solid State Ionics* **1999**, *125*, 39.
(21) Matsushita, E.; Sasaki, T. *Solid State Ionics* **1999**, *125*, 31.
(22) Payne, M. C.; Teter, M. P.; Allan, D. C.; Arias, T. A.; Joannopoulos, J. D. *Rev. Mod. Phys.* **1992**, *64*, 1045.
(23) Jones, R. O.; Gunnarsson, O. *Rev. Mod. Phys.* **1989**, *61*, 689.
(24) Gillan, M. J. In *Computer Simulation in Materials Science*; Meyer, M., Pontikis, V., Eds.; Kluwer: Dordrecht, The Netherlands, 1991.
(25) Perdew, J. P.; Burke, K.; Wang, Y. *Phys. Rev. B* **1996**, *54*, 16533.
(26) Lindan, P. J. D.; Muscat, J.; Bates, S.; Harrison, N. M.; Gillan, M. J. *Faraday Discuss.* **1997**, *106*, 135.
(27) Vanderbilt, D. *Phys. Rev. B* **1990**, *41*, 7892.
(28) Pickard, C. J. Personal communication.
(29) Monkhorst, H. J.; Pack, J. D. *Phys. Rev. B* **1976**, *13*, 5188.
(30) de Vita, A.; Gillan, M. J.; Lin, J. S.; Payne, M. C.; Stich, I.; Clarke, L. J. *Phys. Rev. B* **1992**, *46*, 12964.
(31) Braithwaite, J. S.; Catlow, C. R. A.; Gale, J. D.; Harding, J. H. *Chem. Mater.* **1999**, *11*, 1990.
(32) Ceder, G.; Chiang, Y. M.; Sadoway, D. R.; Aydinol, M. K.; Jang, Y. I.; Huang, B. *Nature* **1998**, *392*, 694.
(33) Koopmans, H. J. A.; van de Velde, G. M. H.; Gellings, P. J. *Acta Crystallogr.* **1983**, *C39*, 1323.
(34) (a) Dravid, V. P.; Sung, C. M.; Notis, M. R.; Lyman, C. E. *Acta Crystallogr.* **1989**, *B45*, 218. (b) Foex, M.; Traverse, J. P.; Coutures, J. *C. R. Acad. Sci., Sér. C* **1967**, *264*, 1837.

Table 1. Calculated and Experimental Structural Parameters of Orthorhombic $CaZrO_3$

(a) Unit Cell Parameters

	experimental[a]	calculated	Δ/%
a (Å)	5.5912	5.5895	−0.03
b (Å)	8.0171	8.0550	0.47
c (Å)	5.7616	5.7667	0.09
V (Å^3)	258.3	259.6	0.50

(b) Atomic Positions, Mean Bond Lengths (in Å), and Bond Angles (in deg)

		experimental[a]	calculated	Δ
Ca	*x*	0.0121	0.0132	0.0011
	y	0.2500	0.2500	0.0000
	z	0.0496	0.0496	0.0000
Zr	*x*	0.5000	0.5000	0.0000
	y	0.0000	0.0000	0.0000
	z	0.0000	0.0000	0.0000
O(1)	*x*	0.6032	0.6101	0.0069
	y	0.2500	0.2500	0.0000
	z	−0.0381	−0.0436	−0.0055
O(2)	*x*	0.3026	0.2998	−0.0028
	y	0.0548	0.0578	0.0030
	z	0.3007	0.2973	−0.0034
Zr−O	(×6)	2.0964	2.1052	0.0088
Ca−O	(×4)	2.3817	2.3742	−0.0075
Ca−O	(×4)	2.7616	2.7680	0.0064
Ca−O	(×4)	3.5101	3.5345	0.0244
Zr−O(1)−Zr		145.76	143.46	−2.30
Zr−O(2)−Zr		146.50	146.35	−0.15

[a] Reference 33.

experiments. Simulation techniques can be used to assist in the identification of the equilibrium position of the proton in the crystal lattice. Several different hydrogen atom positions (bound to an oxygen ion) were thus considered as starting geometries, because there are multiple local minima present.

The lowest energy configuration has the hydrogen atom bound to O(1) with an equilibrium O−H bond distance of 1.01 Å. This suggests that the O(1) site may show a larger proton population than the O(2) site. The predicted OH orientation has the proton site near the direction of a neighboring O(1) ion of an adjacent octahedron (illustrated in Figure 1). It is apparent that a key factor is the tilting of the octahedra in the $CaZrO_3$ structure, which results in short O−O separations between connecting octahedra. The next competitive configuration has the proton bound to O(2) oriented approximately parallel to the ⟨010⟩ axis but with an energy of 0.09 eV higher than the favored O(1)H configuration. These results confirm that the O(1) and O(2) site energies are inequivalent, which will have an influence on the pathway for proton migration.

Analysis of the relaxed structure indicates that the O(1)H hydroxyl species causes small perturbations in the local environment. The hydrogen-bond interaction between the proton and adjacent oxygen ions leads to local changes in nearest-neighbor separations; for example, the nearest-neighbor O−O separation of 3.27 Å reduces to 2.75 Å for O(1)H−O, whereas the O(1)H−Zr distance increases from 2.11 to 2.30 Å.

There are limited structural data on $CaZrO_3$ for direct comparison, although recent muon spin relaxation (μSR) experiments[35] on Sc-doped $SrZrO_3$ find that the muon position does not lie either within the octahedron or along the O−O connection line. Their results also indicate that the positive muon, which acts as a radioactive tracer for the proton, is temporarily trapped at the dopant ion, a topic we return to below. We note that the type of O−H geometry predicted for $CaZrO_3$ may be less important for cubic $BaZrO_3$ in view of the larger unit cell and the absence of octahedral tilting. This is borne out from recent neutron diffraction studies of the pseudocubic systems $BaCeO_3$[8b] and $SrTiO_3$[36] and with our previous simulations[37] of $SrTiO_3$, in which the OH orientation was found to be just off the O−O connection line of the octahedron edge.

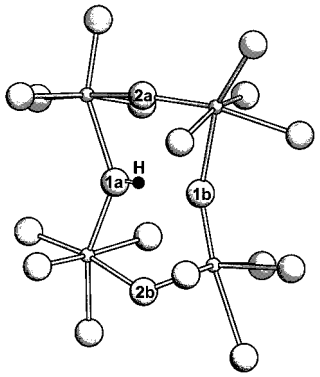

Figure 1. Segment of orthorhombic $CaZrO_3$ showing the ZrO_6 octahedra and the energetically favorable ground-state configuration of the OH species. (The labeling scheme used in this work is indicated.)

3.2. Dynamics of Proton Diffusion. The DFT pseudopotential approach can also be utilized to perform ab initio dynamics which essentially combines the solution of the electronic structure with classical molecular dynamics (MD) for the nuclei. In this work the wave function is optimized to the electronic ground state at every point, as opposed to the fictitious mass dynamics approach by Car and Parrinello.[38] The MD simulations, which are highly computationally demanding, used a periodically repeated system of $Ca_4Zr_4O_{12}H$ and a plane-wave cutoff of 360 eV. Because our main concern here is mechanistic information, these parameters ensure qualitative agreement with our higher accuracy calculations while improving computational efficiency. The simulations used a time step, Δt, of 0.5 fs with a total duration of 4000 time steps (2 ps) at a temperature of 1000 K within the NVT ensemble using a Nosé−Hoover[39] thermostat.

Of primary interest here is the information on the microscopic mechanism revealed by the MD calculations as well as assurance that the true global energy minimum was located in the previous section. Graphical analysis of the evolution of the system with time shows proton-hopping events during the simulation run. Figure 2 presents "snapshots" of one of these proton hops between neighboring O(1) oxygen ions illustrating both initial and barrier (transition) states. This confirms that proton conduction occurs via a simple transfer of a proton from one oxygen ion to the next (Grötthuss

(35) Hempelmann, R.; Soetratmo, M.; Hartmann, O.; Wappling, R. *Solid State Ionics* **1998**, *107*, 269.
(36) Sata, N.; Hiramoto, K.; Ishigame, M.; Hosoya, S.; Nimura, N.; Shin, S. *Phys. Rev. B* **1996**, *54*, 15795.
(37) Cherry, M.; Islam, M. S.; Gale, J. D.; Catlow, C. R. A. *J. Phys. Chem.* **1995**, *99*, 14614.
(38) Car, R.; Parrinello, M. *Phys. Rev. Lett.* **1985**, *55*, 2471.
(39) (a) Nosé, S. *Mol. Phys.* **1984**, *52*, 255. (b) Hoover, W. G. *Phys. Rev. A* **1985**, *31*, 1695.

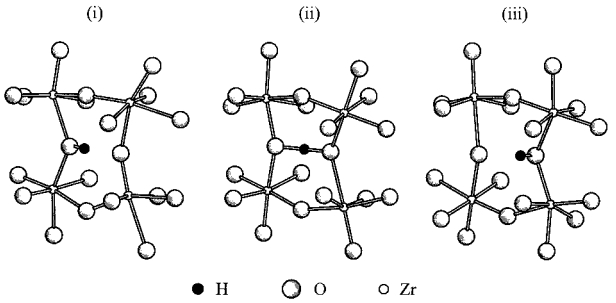

Figure 2. Sequence of three snapshots from ab initio MD simulations showing interoctahedra proton hopping in orthorhombic $CaZrO_3$. (The Ca ions are omitted for clarity.)

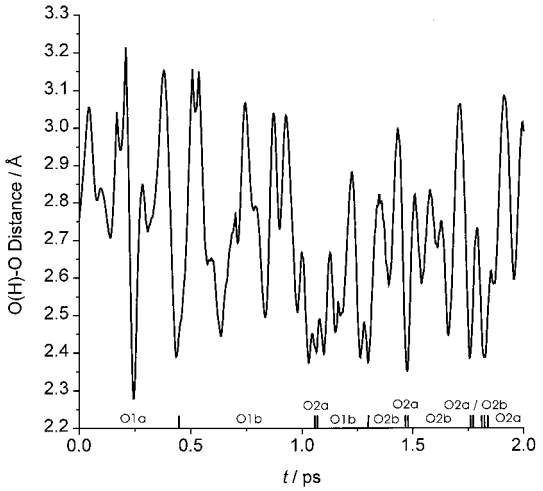

Figure 3. Variation in the interatomic distance between adjacent oxygen ions involved in proton transfer during the ab initio MD simulation.

mechanism). We note that the present simulations provide no evidence for the migration of hydroxyl ions ("vehicle" mechanism) or the existence of "free protons" as proposed by Fillaux,[40] at least on the time scale sampled. However, even with improved statistical sampling of the transition path, this is extremely unlikely to change.

We also find rapid rotational and stretching motion of the O−H group, which allows the reorientation of the proton toward the next oxygen ion before the transfer process. However, the simulations reveal predominantly interoctahedra proton hopping rather than within octahedra. This diffusion path is influenced by the $[ZrO_6]$ tilting within the orthorhombic structure of $CaZrO_3$, which leads to close oxygen−oxygen separations between the vertexes of adjacent octahedra (shown in Figure 2). These results are consistent with the observation that proton mobilities are lower in perovskite structures deviating strongly from cubic.[2] We note that, although in reality there will be a significant contribution of tunneling to assist proton migration, this is unlikely to alter the basic picture because the tunneling rate will be greatest along the direction of lowest activation energy.

Figure 3 plots the variation in O(H)−O distance between adjacent oxygens involved in proton transfer over the course of the MD simulation. This clearly shows the considerable lattice vibrational dynamics with large amplitudes of displacement of the oxygen ions. In particular, for each hopping event the O(H)−O distance shortens from equilibrium values (of 2.75−2.91 Å) to less than 2.4 Å so as to facilitate proton transfer. These simulations, therefore, indicate the importance of oxygen lattice dynamics and suggest that proton transfer is phonon-assisted. We note that recent simulations of zeolites have found similar coupling between proton motion and framework dynamics.[41]

3.3. Proton-Transfer Energetics. In addition to the dynamics calculations, it is possible to derive more quantitative information on the energetics of the individual proton-hopping events. A series of accurate static simulations were carried out to explore systematically the potential energy profile for proton migration between adjacent oxygen sites. This approach allows the identification of the adiabatic energy barrier to proton transfer.

Because the O(1)H site was found to be the most favorable configuration, we have focused our attention on O(1)-mediated mechanisms, namely, O(1)−O(1) and O(1)−O(2) paths. When the position of the proton is kept constant along the oxygen−oxygen path in one dimension and the first oxygen ion is fixed to prevent translation of the entire system, it is possible to optimize the proton position in the two remaining degrees of freedom along with all of the surrounding ions. For instance, in the case of the O(1)−O(1) interoctahedra path, the proton is constrained along the *z* direction directly between the two oxygen ions but is allowed to optimize in the *xy* plane. In this way it is possible to construct the energy profile for the proton-transfer process and identify the barrier state configuration.

The calculated energy profiles are shown in Figures 4−6 for the O(1a)−(O1b), O(1a)−O(2a), and O(1b)−O(2a) paths, respectively, which follow increasing oxygen−oxygen distance; the calculated O−O and O−H interatomic separations as a function of the migration coordinate are also illustrated in these figures. We note that the small energy difference between O(1a) and O(1b) in Figure 4 is due to the small variation in the initial and final OH configurations within the distorted orthorhombic structure. Table 2 lists the barrier energies to proton transfer as well as the initial and barrier state O−O separations derived from the simulations.

Examination of the results reveals that the lowest energy path for proton transfer is the O(1a)−O(1b) interoctahedra jump. This mechanism accords with the MD simulations, which show predominantly proton hopping between octahedra. However, for long-range proton conduction in orthorhombic $CaZrO_3$ comprised of two inequivalent oxygen sites, the rate-limiting step may be the O(1)−O(2) proton transfers with higher energy barriers of up to 0.74 eV (Table 2). This would help to rationalize the high experimental activation energy (>0.7 eV)[44] and relatively low proton conductivity found for doped $CaZrO_3$.

(40) Fillaux, F.; Leygue, N.; Baddour-Hadjean, R.; Parker, S.; Colomban, Ph.; Gruger, A.; Regis, A.; Yu, L. T. *Chem. Phys.* **1997**, *216*, 281.

(41) Fois, E.; Gamba, A. *J. Phys. Chem. B* **1999**, *103*, 1794.
(42) Flynn, C. P.; Stoneham, A. M. *Phys. Rev. B* **1970**, *1*, 3966.
(43) Stoneham, A. M. *J. Chem. Soc., Faraday Trans.* **1990**, *86*, 1215.
(44) Kurita, N.; Fukatsu, N.; Ito, K.; Ohashi, T. *J. Electrochem. Soc.* **1995**, *142*, 1552.

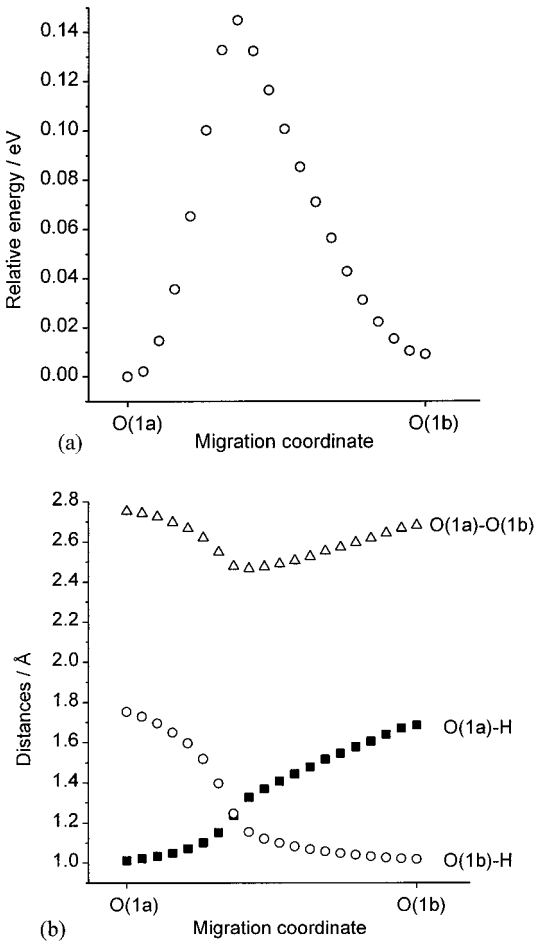

Figure 4. Proton migration along the O(1a)−O(1b) path: (a) energy profile; (b) interatomic distances.

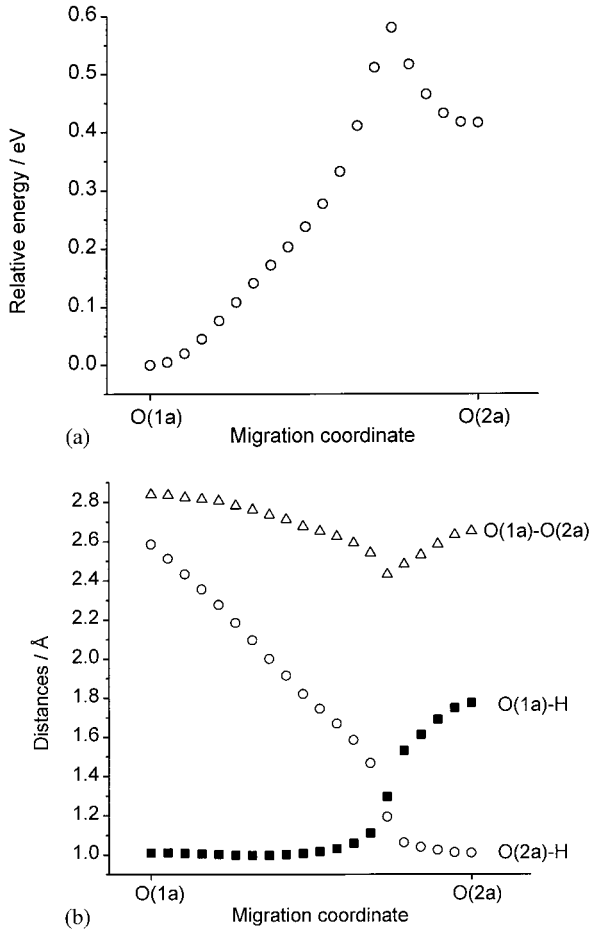

Figure 5. Proton migration along the O(1a)−O(2a) path: (a) energy profile; (b) interatomic distances.

The low barrier energy for the O(1)−O(1) path is consistent with our previous studies,[15,37] where it was suggested that quantum tunneling effects are likely to be important for proton transfer and that a relaxation term is required to acquire the equivalent lattice environments for the two oxygen sites. This idea is analogous to hydrogen interstitial diffusion in metals where quantum effects are known to be important.[42,43] The relaxation effect is predicted to favor high-symmetry structures containing equivalent oxygen sites as in cubic perovskites (e.g., $BaZrO_3$). This avoids extra terms associated with energy differences between nonequivalent sites. A more detailed treatment of quantum tunneling effects is a subject for future investigation.

The variation in interatomic distances as the proton migrates (shown in Figures 4−6) again demonstrates the appreciable modulation of the local lattice associated with proton motion. The shortest O−H bond distance gradually increases toward the barrier state but never extends beyond 1.25 Å. Moreover, analysis of the initial and barrier state O−O distances (Table 2) indicates that in each case the separation reduces to below about 2.5 Å as we found from the MD simulations. This concerted movement of the oxygen ions assists the proton-transfer process by stabilizing the transition state.

The interaction between oxygen ions and the proton is probed further by analysis of the electron density distribution (illustrated as contour maps for the low-energy O(1)−O(1) path in Figure 7). Two main features emerge. First, the hydrogen in the initial state is strongly bonded to an O(1) oxygen ion to form the hydroxyl species. The host lattice also exhibits localized spherical electron density about the nuclei indicative of the largely ionic character. Second, the barrier state clearly displays a symmetric density distribution, in which there is equal hydrogen bonding to the two adjacent oxygen ions (leading to a shorter oxygen−oxygen distance). This confirms that the proton is not transferred through a totally "free" state, so that all of the OH bonds are never completely broken.

3.4. Proton−Dopant Interactions. The addition of aliovalent dopants is crucial to proton dissolution. The $CaZrO_3$ material is typically acceptor-doped with trivalent ions (e.g., In^{3+}) at the Zr^{4+} site. However, it is still not clear whether there is any significant interaction between the protonic defect and the dopant ion, leading to association or proton "trapping". Kreuer et al.[2,16] suggest that the observed increase in activation energy for proton diffusivity in $BaCeO_3$ with increasing dopant content may be related to the general increase of the oxygen basicity and the proton-transfer barrier. In contrast, μSR measurements of Hempelmann et al.[35] on Sc-doped $SrZrO_3$ suggest that, in the course of their diffusion, protons are temporarily trapped at single dopant ions. Quasi-elastic neutron scattering (QENS) studies[45] on doped $SrCeO_3$ also suggest the presence of

(45) Karmonik, C.; Hempelmann, R. *Phase Transitions* **1996**, *58*, 175.

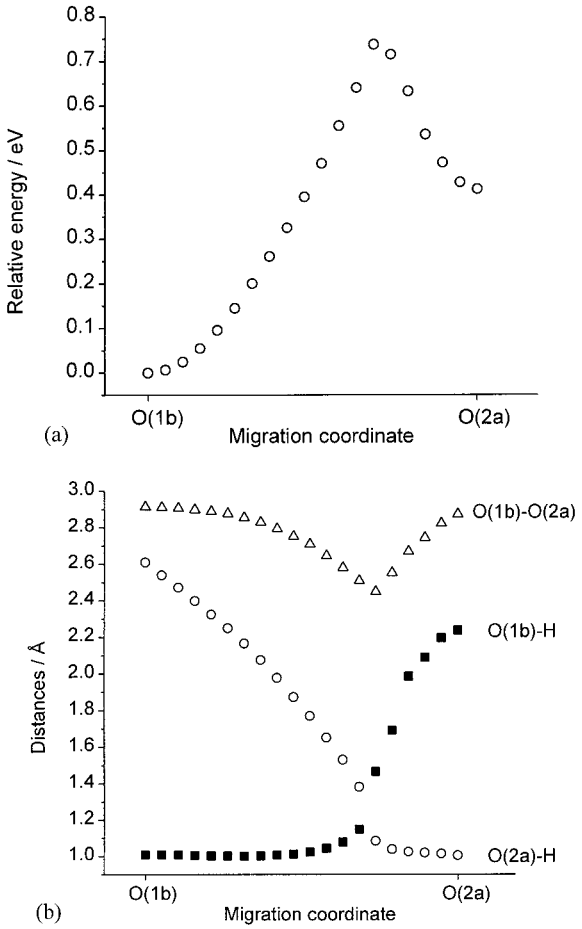

Figure 6. Proton migration along the O(1b)−O(2a) path: (a) energy profile; (b) interatomic distances.

Table 2. Barrier Energies to Proton Transfer and Oxygen−Oxygen Separations for the Initial and Barrier State Configurations

migration path[b]	E_b/eV[a]	O−O(initial)/Å	O−O(barrier)/Å
O(1a)−O(1b)	0.14	2.75	2.48
O(1a)−O(2a)	0.58	2.84	2.43
O(1b)−O(2a)	0.74	2.91	2.51

[a] 1 eV ≡ 96.486 kJ mol^{-1}. [b] Oxygen sites labeled in Figure 1.

a considerable amount of proton associated with the dopant.

In an attempt to probe this problem, we carried out a series of calculations on defect pairs comprised of a hydroxyl ion and a dopant substitutional at nearest-neighbor sites (illustrated in Figure 8). Attention was focused on three commonly used dopants in $CaZrO_3$, namely, Ga^{3+}, Sc^{3+}, and In^{3+}. The same computational parameters are used for the doped material as for the pure phase but with a larger periodically repeated system of 41 atoms (corresponding to $Ca_8Zr_7MO_{24}H$) in order to achieve a lower dopant content. The proton-dopant binding energies are calculated with respect to the energies of the component isolated hydroxyl ion and dopant ion, given by the general expression:

$$E_{\text{bind}} = E_{\text{defect pair}} - \sum E_{\text{isolated defects}} \qquad (1)$$

where a negative value for E_{bind} would indicate that the system is bound. For the calculations of the isolated charged defects, an additional energy term is required

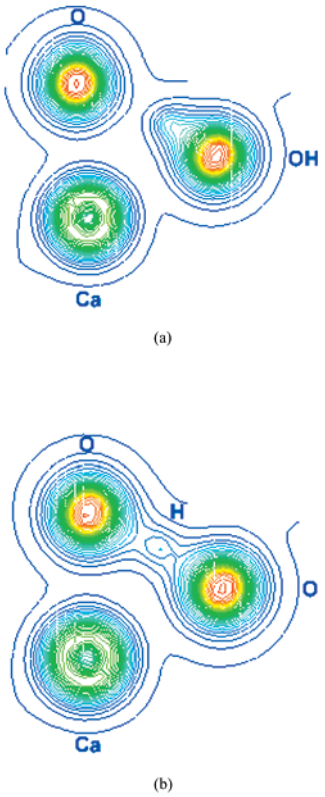

Figure 7. Electronic charge density for O(1a)−O(1b) proton transfer in the plane defined by Ca and O(1) atoms: (a) initial state; (b) barrier state.

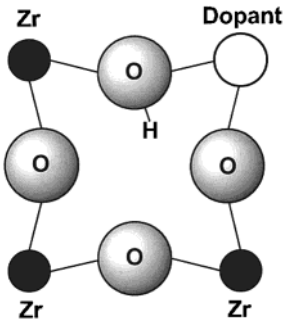

Figure 8. Schematic representation of a hydroxyl−dopant pair at nearest-neighbor sites in orthorhombic $CaZrO_3$.

Table 3. Binding Energies of Hydroxyl−Dopant Pairs ($OH_O^{\bullet}M'_{Zr}$) at Nearest-Neighbor Sites

dopant	E_{bind}/eV
Ga^{3+}	−0.18
Sc^{3+}	−0.31
In^{3+}	−0.30

for the interaction with the uniform neutralizing background charge, as discussed by Leslie and Gillan.[46]

The resulting binding energies (reported in Table 3) reveal that all of the hydroxyl−dopant pairs are predicted to be favorable configurations, with the lowest value for Ga^{3+}. Although there are no experimental data on $CaZrO_3$ for direct comparison, the calculated values accord well with proton "trapping" energies of about −0.2 and −0.4 eV for Sc-doped $SrZrO_3$ and Yb-doped $SrCeO_3$, respectively, derived from recent μSR and QENS experiments.[35,45] The μSR study[35] postulates a

(46) Leslie, M.; Gillan, M. J. *J. Phys. C* **1985**, *18*, 973.

model for muon diffusion involving random sequences of trapping events and free diffusion periods. The present calculations, therefore, predict that the presence of such defect pairs is certainly a possibility in the $CaZrO_3$ material. These results also accord with our previous atomistic simulations[14] on hydroxyl−dopant pairs in doped $SrZrO_3$. It is noted, however, that trapping does not necessarily preclude the presence of isolated protons and dopant ions, because clusters will be in equilibrium with single defects. This picture can be viewed as analogous to oxygen ion conductivity in acceptor-doped fluorite (and perovskite) oxides and the well-known importance of dopant−vacancy interactions.[47−49]

4. Conclusions

A computational study based on DFT methodology has allowed us to probe proton transport in the $CaZrO_3$ orthorhombic perovskite with a high level of microscopic detail. This study forms part of the continuing effort to improve our understanding of proton transport, a key phenomenon in a wide variety of areas that ranges from inorganic solids to biological systems. The following aspects emerge from our work:

(1) The observed orthorhombic crystal structure (comprised of tilting [ZrO_6] octahedra) is reproduced accurately. The equilibrium OH configuration has the proton bound to the apical oxygen O(1) with a bond length of 1.01 Å. The calculations confirm that the O(1) and O(2) site energies are inequivalent, which influences the pathway for proton migration.

(2) Ab initio MD simulations confirm that the diffusion mechanism involves proton transfer from one oxygen ion to the next (Grötthuss-type mechanism). The simulations indicate the importance of vibrational dynamics of the oxygen sublattice and suggest that proton transfer is phonon-assisted. For each hopping event, the oxygen−oxygen distance contracts to about 2.4−2.5 Å so as to facilitate proton transfer by stabilizing the barrier (or transition) state. At this barrier state, the calculated electron density shows equal hydrogen bonding to the two oxygen ions, indicating that the proton is not transferred through a totally "free" state.

(3) A very low energy barrier for proton transfer is found for the O(1)−O(1) interoctahedra path, influenced by the close oxygen−oxygen separations between tilting octahedra. These results support our previous calculations,[37] where it was suggested that quantum tunneling effects are likely to be important for proton transfer and that a relaxation term is required to acquire equivalent lattice environments for the two oxygen sites. Long-range proton conduction in $CaZrO_3$ may, however, involve O(1)−O(2) proton transfer as the rate-limiting step with a calculated energy barrier of 0.74 eV. This agrees with experimental activation energies and may help to rationalize the relatively high energies for proton conductivity in this material.

(4) Binding energies for hydroxyl−dopant pairs (involving Ga^{3+}, Sc^{3+}, and In^{3+} dopant ions) are predicted to be favorable and are compatible with observed proton "trapping" energies for related perovskites from μSR and QENS experiments.

Acknowledgment. We thank EPSRC for funding this work, the Royal Society for a University Research Fellowship (JDG), and the Computational Chemistry Working Party for the facilities at the Rutherford Appleton Laboratory, U.K.

CM010005A

(47) Gerhardt-Anderson, R.; Lee, W. K.; Nowick, A. S. *J. Phys. Chem. Solids* **1987**, *48*, 563.
(48) Catlow, C. R. A. *J. Chem. Soc., Faraday Trans.* **1990**, *86*, 1167.
(49) Kilner, J. A. *Solid State Ionics* **2000**, *129*, 13.